Journal of Materials Chemistry A

Accepted Manuscript

ROYAL SOCIETY OF CHEMISTRY

www.rsc.org/materialsA

Journal Name

ARTICLE

Highly Flexible, Conductive and Catalytic Pt Networks as Transparent Counter Electrode for Wearable Dye-sensitized Solar Cells

Received 00th January 20xx,
Accepted 00th January 20xx

DOI: 10.1039/x0xx00000x

www.rsc.org/

Ranran Zhou[a+], Wenxi Guo[a+], Ruomeng Yu[b], Caofeng Pan[a]*

We present a highly flexible dye-sensitized solar cell composing of TiO_2 nanotube arrays (TNARs) as photoanode and a transparent Pt network electrode as counter electrode (CE). The network-structured Pt electrodes can be transferred onto arbitrary flexible substrates at room temperature and exhibit remarkable mechanical flexibility in bending and twisting tests. Up to 94% transmittance for Pt network electrodes can be obtained when the sheet resistances are over 170 Ω sq^{-1}. The CV and EIS analysis of the Pt networks reveal a comparable electrocatalytic behavior with the thermal deposition Pt particles on FTO glass. A photoelectric-conversion efficiency (PCE) of 3.82% was obtained by utilizing Pt networks as CEs in TNARs based DSSCs and maintained >90% PCE after 200 bending cycles. Such metal networks based electrodes would be widely used not only in flexible solar cells but also in the other wearable, lightweight electronic devices.

1 Introduction

With the development of portable and light-weight electronic products, more and more flexible and even foldable energy harvesting and storage devices are required. Dye-sensitized solar cells (DSSCs), as a low-cost alternative to silicon based solar cells, have attracted extensive attentions in the last two decades due to their easy fabrication and relatively high conversion efficiency.[1-3] Compared with the DSSCs based on rigid and brittle conductive glass, flexible DSSCs possess certain superiorities in weight, volume, transportation, installation and roll-to-roll production. To obtain high-quality crystalline and good adhesive semi-conductive photoanode of the DSSCs, high temperature annealing (up to 450 °C) is usually required,[4, 5] while this process largely restricts the use of the flexible transparent conducting oxide (TCO) plastic substrates. Alternative to the plastic substrates, Ti foil is usually employed as a proper photoanode substrate due to its high flexibility, conductivity and excellent thermal stability. [6, 7] Besides, it is also suitable for large-area fabrication of highly ordered TiO_2 nanotube arrays (TNARs) by electrochemical anodization.[8-10] However, the Ti foils are non-transparent, which limits the configuration of the DSSCs to back-side illumination. Therefore, the counter electrodes (CEs) with good transmittance, high flexibility and excellent catalytic activity are keenly needed.

Among various flexible CEs, platinum (Pt) is an excellent candidate because of its ideal catalytic activity to reduce the redox couple. Several low temperature techniques have been employed to fabricate semi-transparent Pt electrodes on polymer substrates, including sputtering,[11, 12] electrodeposition,[13, 14] atomic-layer-deposition (ALD),[15] and chemical reduction[16] etc. However, some issues still exist in these techniques: Firstly, all the Pt CEs fabricated by the aforementioned techniques require additional indium tin oxide (ITO) film which is brittle and prone to cracking under the bending or torsion force.[17-21] Secondly, the compromise among the transmittance, electrocatalytic activity and cost is difficult to control. For example, directly sputtering Pt onto the flexible substrates is a fast and reliable process, but it will greatly reduce the transmittance.[22, 23] Electrodeposition (ED) can provide transparent CEs but leads to an inhomogeneous distribution of nanoparticles.[24] ALD technique can fabricate highly uniform and transparent Pt CEs, but it is time-consuming and not cost-effective which restricts its industrial production.[25]

Electrospinning[26-28] has been reported as an effective method to fabricate continuous polymer fibers and even transparent electrodes, which has attracted great interests due to the low cost and scalability properties. Among them, Cui's group demonstrates the practical suitability of their transparent conducting gold electrode by fabricating a flexible touch-screen device and a transparent conducting tape; however, up to now, few researchers report about the electrochemical catalytic ability of the electrodes and apply them into the DSSCs. Here, to satisfy all the aforementioned requirements for Pt CEs simultaneously, Pt networks derived

[a] Beijing Institute of Nanoenergy and Nanosystems, Chinese Academy of Sciences, Beijing, 100083, China
[b] School of Materials Science and Engineering, Georgia Institute of Technology, Atlanta,Georgia 30332-0245, USA
† Authors contributed equally to this work.
Electronic Supplementary Information (ESI) available: [supplementary video1 and 2]. See DOI: 10.1039/x0xx00000x

from electrospinning poly (vinyl alcohol) (PVA) nanofibers and sputtering Pt were developed as CEs for the TNARs based DSSCs. The Pt network electrodes not only serve as conducting film, but also exhibit excellent transmittance (sheet resistance of 100~150 Ω sq^{-1} at about 80%~85% transmission) and similar catalytic activity in the reduction of I_3^- in DSSCs to that of the thermal evaporated Pt. Furthermore, the network electrodes could be constructed on arbitrary flexible substrates at room temperature. After bending tests, the Pt network CEs and those based DSSCs demonstrated remarkable mechanical stability. The highest efficiency of ~3.82% was obtained by utilizing Pt networks as CEs in the TNARs based DSSCs.

2 Experimental

2.1 Preparation of photoanode

A thin-film titanium (Ti) foil (ca. 30μm) was pre-cleaned by acetone, alcohol and deionized water, then the highly ordered TNARs were fabricated on Ti foil by electrochemical anodization.[29] The obtained TNARs/Ti foil was annealed at 450 °C in oxygen for 2 h with heating and cooling rates of 5 °C/min to induce crystallinity. After annealing, the sample was subsequently treated in 20 mM $TiCl_4$ solution for 30 min at 75 °C and then further annealed at 450 °C for 30 min. The commercially available ruthenium based dye $RuL_2(NCS)_2$:2TBA (N-719) was used as the sensitizer, with the concentration of 0.3mM in ethanol. The TNARs/Ti foils samples were immersed in N-719 for 24 h to form a photoanode. The microstructure of the fabricated TiO_2 nanotubes was characterized through scanning electron microscope (SEM) (Hitachi SU 8020).

2.2 Preparation and characterization of CE

The CE was fabricated through electrospinning of PVA nanofibers. After the electrospinning, Pt nanoparticles were sputtered on the PVA nanofibers by magnetron sputtering at room temperature, with the flow rate of argon at 100 sccm, with sputtering power of 100 W for 3 minutes. After spritzing some deionized water onto the flexible substrates, the resulting Pt nanofibers were then transferred to the substrates and baked at 70 °C for 2 minutes to dry out. To completely remove the PVA nanofibers, the samples were dipped into deionized water for 10 minutes and then dried at 70 °C, this process can be repeat several times to obtain the proper resistance.

A digital multimeter (Keithley 2100) with a four-point probe was used to measure the films' sheet resistances. The light transmittance of the hybridized electrodes was measured by UV-vis spectroscopy (Shimadzu UV-3600). To examine mechanical durability, the electrode was bent by a motor, and released to the initial position. Electrochemical performance measurements of the fabricated Pt networks were performed using an Autolab electrochemical workstation (Autolab, PGSTAT30, Metrohm), in the conventional three-electrode system.

2.3 Device fabrication

For the fabrication of DSSCs, the aforementioned photoanode was then assembled with the Pt CE using a 25 μm thick hot-melt sealed film as the spacer (SX1170-25; Solaronix Co.), then these two electrodes were fixed with clips and heated to 120

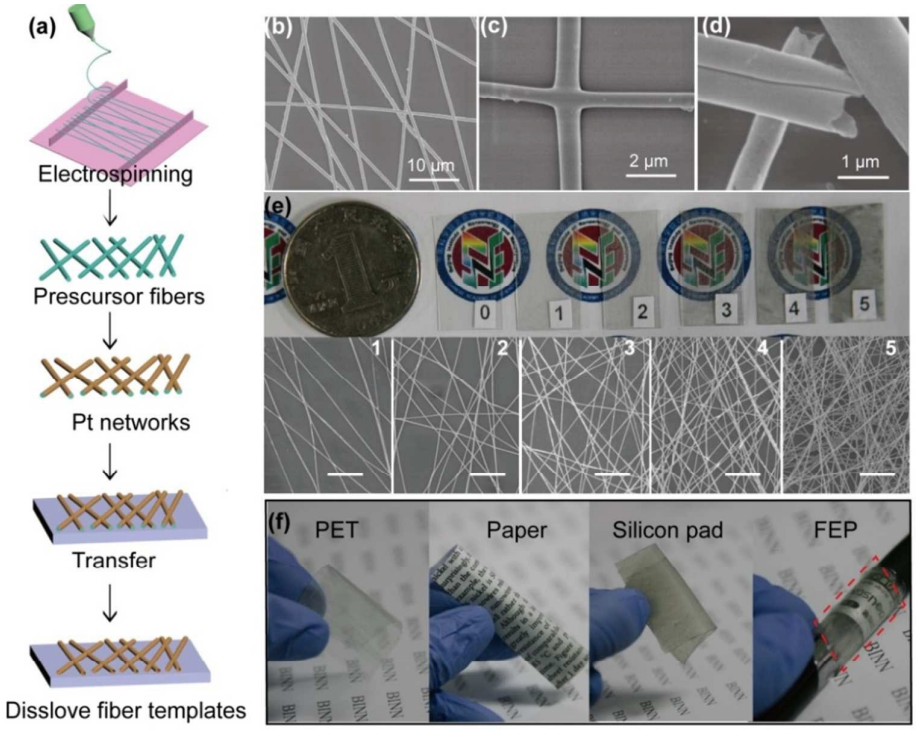

Fig.1 (a) 3D schematic diagram of PVA nanofiber templating process for fabricating Pt networks. (b) (c) and (d) are SEM images Pt networks in different magnification. (e) Photographs of Pt networks with different transmittance and their corresponding SEM images (Scale bar: 20 μm). (f) Photographs of Pt networks on different substrates, including PET, Paper, Silicone pad, and FEP (left to right).

°C for 3min to stick them together. The electrolyte including 0.5 M LiI, 50 mM I_2, and 0.5 M 4-tert-butylpyridine in 3-methoxypropionitrile was injected into the cells by capillary effect. The active area of the prepared solar cell was (0.2cm*1cm). A Solux solar simulator calibrated with a Daystar meter was used to simulate sunlight for an illumination intensity of 100 mW cm^{-2}. The solar cell was irradiated using a solar simulator (SOLO22A, CROWTECH) with an AM 1.5 spectrum distribution calibrated against an NREL reference cell to simulate accurately a full-sun intensity (100 mW cm^{-2}). The incident photon-to-current efficiency (IPCE) spectra were measured by a monochromator (Oriel, Model: 74125).

3 Results and discussion

3.1 Fabrication process of the Pt networks

The 3D schematic diagram in Figure 1a presents the fabrication and transfer process of the Pt networks. Firstly, continuous PVA nanofibers were fabricated through electrospinning. Secondly, the random PVA networks were coated with Pt thin film by utilizing magnetron sputtering technique. This low temperature deposition technique can be used to sputter various metal films and retaining the bulk-like electrical conductivity. Thirdly, the as-fabricated Pt@PVA networks were transferred onto different substrates and the hollow structured Pt networks were derived after removing the PVA nanofibers by dipping them into the deionized water.

The microstructure of the fabricated Pt networks with different sheet resistances are characterized by SEM. Figure 1b shows a typical example of the Pt network electrodes, the diameters of the Pt networks vary from 200 nm to 600 nm, which can be controlled by adjusting the electrospinning parameters. Figure 1c presents the interlaced Pt networks, which shows a good fused junction. The enlarged SEM in Figure 1d shows the hollow structure of the networks, indicating the dissolution of the PVA nanofibers. Figure 1e presents the as-prepared CEs with different transmittance on the PET substrates and their corresponding SEM images. It is obvious to see that the density of the Pt networks increased with a decrease of the transmittance. Figure 1f exhibits some examples that Pt networks are successfully transferred onto various substrates, including polyethylene terephthalate (PET), paper, silicone pad and fluoroethylene polymer (FEP) respectively. The networks are firmed attached onto the substrates and can endure bending or twisting for hundreds of times without peeling off.

3.2 Mechanical properties of the Pt network electrodes

The mechanical flexibility of the Pt networks was further tested in terms of periodically bending. Figure 2a shows the sheet resistances of Pt networks on PET as a function of the bending cycles at a bending radius of 1.134 cm (2.4 cm*1.0 cm), the measurement setup including a motor and a fixed displacement platform is shown in the inset. Here, we chose Pt networks with resistance of 80Ω/sq as an example, which is comparable with ITO electrodes (70Ω/sq). No obvious degradation in electrical conductivity is observed for Pt networks, while the sheet resistance of the commercialized ITO/PET films increases about 6-fold after 1000 bending cycles. The poor stability of the ITO is mainly due to the brittle and fragile ceramic structure tends to crack during bending or twisting, while the nanotrough networks remain continuous and can undergo nanoscale deformation without fracturing.[28] Furthermore, we also tested the mechanical properties of the Pt networks under extreme conditions by transferring them on the super-thin FEP film. Figure 2b shows the I-V curves of the Pt networks on FEP film during the factitious twisting and folding. Comparing with the initial state (black line), the twisting state shows a slight current decrease. After crushing, twisting and unfolding for several times, the electrode remains its conductivity (Supplementary Video1). The huge advantage of the metal networks is of great importance in transparent conductive applications. This electrospinning technique can be employed to fabricate various highly durable metal networks and probably enable the development of wearable and lightweight optoelectronic devices.

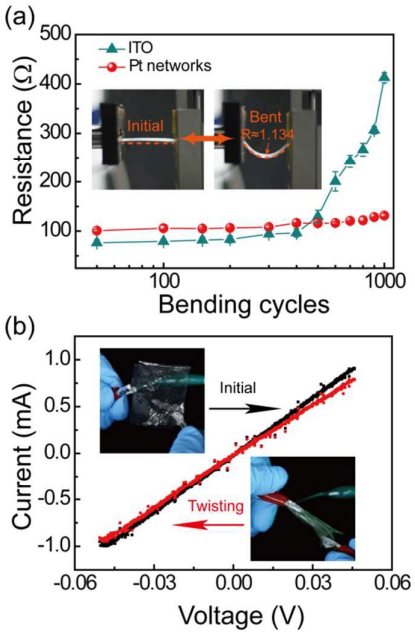

Fig. 2 (a) Resistance measurements of Pt networks and ITO both on PET substrates under the repeated bending condition. (b) I-V curve for the Pt networks on FEP substrate (black) and in the twisting case (red).

3.3 Electrocatalytic properties of the Pt network electrodes

Figure 3a shows the UV-vis spectra of as-prepared Pt networks on PET substrates, and the commercialized ITO and FTO glass as a comparison. All the Pt networks with different resistance demonstrate flat transmittance spectra for the entire wavelength range from 400 nm to 2000 nm, while a sharp decrease in the range of wavelength greater than 1000 nm for both the FTO and ITO electrodes, indicating their low transmittance in the infrared spectrum. The inset in Figure 3a presents the sheet resistances of Pt networks versus optical

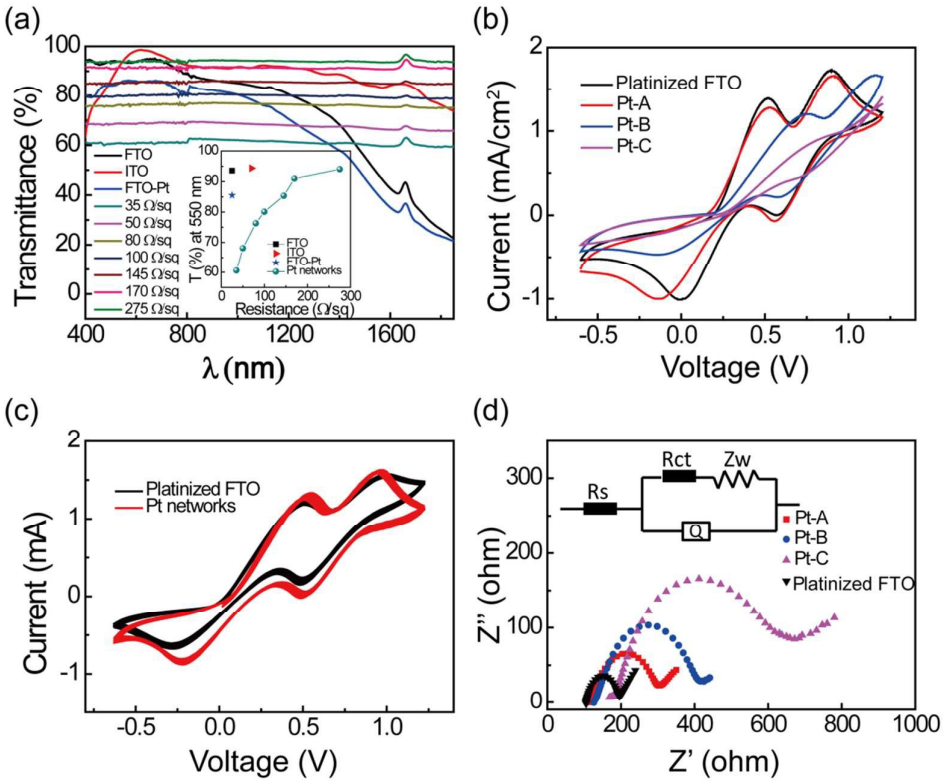

Fig. 3 (a) UV-vis spectra of FTO glass, ITO, Platinized FTO and Pt networks. Inset: Resistance versus optical transmission (fixed at 550 nm) for the different CEs. (b) Cyclic voltammetry (C-V) curves of Platinized FTO and Pt networks with different resistances. (c) C-V stability tests of Platinized FTO and Pt networks after 50 scanning cycles. (d) Nyquist plots of Platinized FTO and Pt networks with different resistances.

transmission at 550 nm. Obviously, with increasing the sheet resistance of the Pt networks films, the transmittance increased as expected, and up to 94% optical transmittance was achieved when the sheet resistance was about 275 Ω sq^{-1}. To systematically elucidate the relationship among sheet resistance, transmittance and electrochemical catalytic activity, we chose three typical samples from all the Pt network electrodes according to their sheet resistance: ~40 Ω sq^{-1}, ~140 Ω sq^{-1} and ~250 Ω sq^{-1}, where Pt-A, Pt-B and Pt-C were represented for the three typical samples, respectively.

To better recognize the electrochemical catalytic activity of the Pt networks for the reduction of triiodide, electrochemical measurements were performed and the results are shown in Figure 3(b-d). Cyclic voltammetry (CV) curves of various CEs in triiodide electrolyte were investigated from -0.6 V to 1.2 V at a scan rate of 50 mV s^{-1}, as plotted in Figure 3b. Here, as a comparison, semi-transparent platinized FTO glass obtained by means of thermal decomposition (400 °C) was introduced. All Pt network CEs show two pairs of oxidation and reduction peaks similar to that of the thermal evaporated Pt particles. The relative negative pair on the left was attributed to the redox reaction of $I_3^- + 2e^- = 3I^-$, while the right pair resulted from the reaction $3I_2 + 2e^- = 2I_3^-$.[30-32] As expected, the reduction peak currents increased with increasing the density or decreasing the sheet resistance of the Pt networks. The catalytic ability was similar to platinized FTO glass when the sheet resistance of Pt networks was ~40 Ω sq^{-1}. Furthermore, the electrochemical stability of the Pt network CE was as well tested by measuring successive CV plots with 50 cycles. As can be observed from Figure 3c that the CV stability of the Pt networks is similar to the platinized FTO, and there is only an 8.9% increase in the cathodic peak current density and a 5.55% decrease in the anodic peak current density from the first to 50th CV curves for the Pt networks sample, which indicates a superior stability of the prepared Pt networks.

The catalytic performance of as-prepared Pt networks was evaluated by electrochemical impedance spectroscopy (EIS) measurements using a symmetric cell configuration. The results and the corresponding circuit model are shown in Figure 3d, the fit parameters are listed in Table 1 by using the standard model. All the Nyquist plots exhibit a semicircle and a diagonal line with slope of 45° corresponding to the charge transfer resistance (R_{ct}) at high frequencies and Warburg impedance from the electrolyte diffusion at low frequencies, respectively. The series resistance and the charge transfer resistance of the samples (Pt-A to Pt-C) monotonically increase with increasing the sheet resistances of the Pt networks, which

totally agrees with the tendency of the corresponding reduction current density in Figure 3b.

Table 1. Performance parameters of the DSSCs with different Pt CEs.

Sample	R_s (Ω)	R_{ct} (Ω)	V_{oc} (V)	J_{sc} (mA cm^{-2})	FF	η (%)
Pt-A	115	189.8	0.58	9.6	0.472	2.63
Pt-B	130.2	286.1	0.66	10.99	0.53	3.82
Pt-C	176.4	482.3	0.66	10.95	0.48	3.47
Pt/FTO	106.1	86.96	0.65	11.36	0.56	4.13

3.4 Characterization of the DSSCs

Figure 4a represents a digital photo and the corresponding three-dimensional schematic structure of a flexible DSSC, in which the highly ordered TiO_2 nanotube arrays (TNARs) were employed as photoanode materials, as shown in Figure 4b and c. The highly transparent and flexible Pt networks with various sheet resistances were applied as the CEs. Figure 4d shows typical plots of the current density versus voltage for the DSSCs with Pt-A, Pt-B, Pt-C and platinized FTO, under AM 1.5 solar simulator illumination at 100 mW cm^{-2}. The performance of The TNARs based DSSCs with Pt networks CEs are ruled by a compromise among the conductivity, transmittance and the electrocatalytic activity. The DSSC using Pt-A CE shows a lowest open-circuit voltage (V_{oc}) of 0.57 V and short-circuit current (J_{sc}) of 9.6 mA cm^{-1} while the DSSC using Pt-B CE shows a V_{oc} of 0.68 V and J_{sc} of 10.99 mA cm^{-1}, and the photoelectric-conversion efficiency (PCE) increases from 2.63% to 3.82%. A higher efficiency was achieved in Pt-B mainly due to the significant increase of the light transmittance (20%, ca. from 65% to 85%). However, the PCE demonstrates a little decrease as the sheet resistance further increasing to ~250 Ω sq^{-1} (Pt-C). Although Pt-C exhibits the highest transmittance, the decrease of the Pt loading would cause a lower FF and consequently a lower efficiency. Therefore, it is important to take a balanced point between the resistance and transmittance, which has been elaborated in Figure 3.

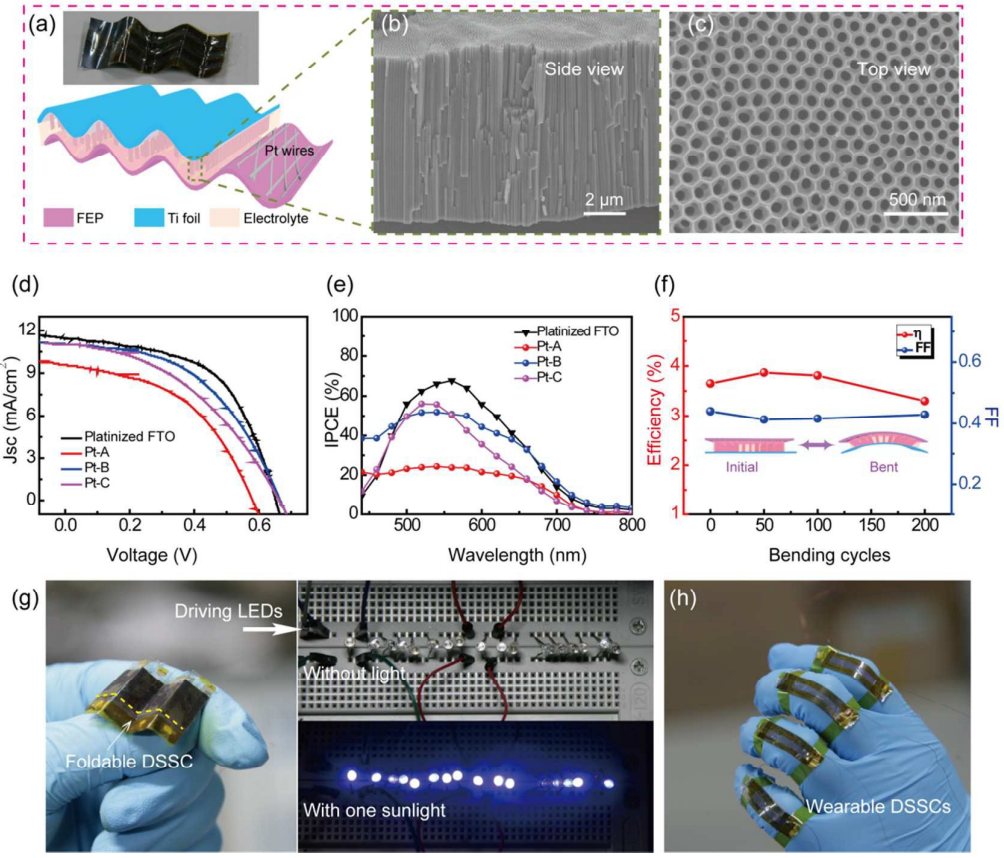

Fig.4 Characteristics of the fabricated Pt networks based DSSC. (a) 3D schematic diagram of the fabricated DSSC. (b) Side view and (c) top view of the SEM image of the TiO_2 nanotubes. (d) J-V curves and (e) Incident photon to current conversion efficiency (IPCE) of the fabricated DSSCs with different CEs. (f) Stability measurements of the flexible DSSC after periodical bending. (g) Driving LEDs measurements of the foldable DSSCs. Photographs of the prepared DSSC and the LEDs with and without sunlight exposed on the DSSC. (h) Photograph of the wearable DSSCs affixed to the human fingers.

These results can be further confirmed by the corresponding incident photo-to-current conversion efficiency (IPCE) measurements shown in Figure 4e. It is obvious that the IPCE values of the sample Pt-B and Pt-C based DSSCs are much larger than that of the Pt-A, which is agree with the tendency of the corresponding values of J_{sc} and PCE. Although the IPCE value of Pt-B based DSSCs in the wavelength of 500-550 nm is slightly smaller than Pt-C, Pt-B exhibits better performance in the rest of wavelength band, which is second only to the platinized FTO glass based DSSC. Furthermore, in order to investigate the mechanical flexibility of the DSSCs based on Pt networks electrodes, periodic bending tests were performed. Figure 4f presents the values of PCE and FF as a function of the bending cycles. The inset 3D diagram shows the measurement state of the devices. Only 9.6% decrease in PCE (from 3.65% to 3.3%) after 200 times bending cycles. The excellent tolerance towards repeated mechanical deformation can promote its applications in the field of lightweight and wearable solar cells.

Moreover, the prepared foldable DSSC can be employed to drive the blue LEDs, which can be seen in Figure 4g. Here, the solar cell was prepared on the PET substrates, so that it could be folded easily. A row of LEDs were plugged onto the breadboard in parallel. As the sunlight exposed on the DSSC, the parallel LEDs were lit up immediately (Supplementary Video2). This process can be repeated for several times, without any brightness diminishment of the LEDs. Figure 4h exhibits four wearable DSSCs were adhered onto the human fingers. To obtain the highly flexible and wearable solar cells here, the Pt networks were transferred onto the transparent FEP substrates, which also possessed a super-thin property. On this basis, the solar cells could be prepared into various shape and size, which would be of great importance in the practical wearable applications.

4 Conclusion

In this study, we have elaborated a simple and cost-effective approach to fabricate flexible and transparent Pt network electrodes, which exhibit both excellent optoelectronic properties and remarkable mechanical stability. The CV and EIS analysis of the Pt networks reveal a comparable electrocatalytic behavior with the platinized FTO electrodes. The DSSCs based on Pt networks show a robust property against mechanical bending, which maintain >90% PCE after 200 bending cycles. Besides, the Pt networks can be transferred onto arbitrary substrates at room temperature, which makes it possible to fabricate wearable, lightweight and conductive textiles or films. Such metal networks based electrodes would have a great potential application in lightweight photovoltaic fields and other smart and portable electronic products area.

Acknowledgements

The authors thank for the support from the "thousands talents" program for pioneer researcher and his innovation team, China; President Funding of the Chinese Academy of Sciences, National Natural Science Foundation of China (No.51272238, 21321062, 51432005 and 61405040), the Innovation Talent Project of Henan Province (No.13HASTIT020), Talent Project of Zhengzhou University (ZDGD13001) and Surface Engineering Key Lab of LIPCA.

Notes and references

1 B. Oregan and M. Gratzel, *Nature*, 1991, **353**, 737-740.
2 A. Yella, H. W. Lee, H. N. Tsao, C. Y. Yi, A. K. Chandiran, M. K. Nazeeruddin, E. W. G. Diau, C. Y. Yeh, S. M. Zakeeruddin and M. Gratzel, *Science*, 2011, **334**, 629-634.
3 S. Mathew, A. Yella, P. Gao, R. Humphry-Baker, F. E. CurchodBasile, N. Ashari-Astani, I. Tavernelli, U. Rothlisberger, K. NazeeruddinMd and M. Grätzel, *Nat. Chem.*, 2014, **6**, 242-247.
4 B. Liu and E. S. Aydil, *J. Am. Chem. Soc.* , 2009, **131**, 3985-3990.
5 K. Yan, Y. Qiu, W. Chen, M. Zhang and S. Yang, *Energy Environ. Sci.*, 2011, **4**, 2168-2176.
6 L. Y. Lin, C. P. Lee, R. Vittal and K. C. Ho, *J. Power Sources* 2010, **195**, 4344-4349.
7 J.-Y. Liao, B.-X. Lei, H.-Y. Chen, D.-B. Kuang and C.-Y. Su, *Energy Environ. Sci.*, 2012, **5**, 5750-5757.
8 M. Ye, X. Xin, C. Lin and Z. Lin, *Nano Lett.*, 2011, **11**, 3214-3220.
9 G. K. Mor, K. Shankar, M. Paulose, O. K. Varghese and C. A. Grimes, *Nano Lett.*, 2006, **6**, 215-218.
10 M. Ye, D. Zheng, M. Lv, C. Chen, C. Lin and Z. Lin, *Adv. Mater.*, 2013, **25**, 3039-3044.
11 L.-Y. Lin, M.-H. Yeh, K.-W. Tsai, C.-Y. Chen, C.-G. Wu and K.-C. Ho, *Electrochem. Commun.* , 2013, **37**, 71-75.
12 B. Yoo, M. K. Lim and K.-J. Kim, *Curr. Appl. Phys.*, 2012, **12**, 1302-1306.
13 S.-S. Kim, Y.-C. Nah, Y.-Y. Noh, J. Jo and D.-Y. Kim, *Electrochimica. Acta*, 2006, **51**, 3814-3819.
14 N. Fu, X. Xiao, X. Zhou, J. Zhang and Y. Lin, *J. Phys. Chem. C*, 2012, **116**, 2850-2857.
15 D. Garcia-Alonso, V. Zardetto, A. J. M. Mackus, F. De Rossi, M. A. Verheijen, T. M. Brown, W. M. M. Kessels and M. Creatore, *Adv. Energy Mater.* , 2014, **4**, 1300831.
16 H. Lu, D. Zhang, X. Ren, J. Liu and W. C. H. Choy, *ACS Nano*, 2014, **8**, 10980-10987.
17 D. R. Cairns, R. P. Witte, D. K. Sparacin, S. M. Sachsman, D. C. Paine, G. P. Crawford and R. R. Newton, *Appl. Phys. Lett.*, 2000, **76**, 1425-1427.
18 D. S. Hecht, L. Hu and G. Irvin, *Adv. Mater.*, 2011, **23**, 1482-1513.
19 D. R. Cairns and G. P. Crawford, *Proc. IEEE*, 2005, **93**, 1451-1458.
20 K. A. Sierros, N. J. Morris, K. Ramji and D. R. Cairns, *Thin Solid Films*, 2009, **517**, 2590-2595.
21 A. D. Azar, E. Finley and K. D. Harris, *Rev. Sci. Instrum.*, 2015, **86**, 013901.
22 Y.-L. Lee, C.-L. Chen, L.-W. Chong, C.-H. Chen, Y.-F. Liu and C.-F. Chi, *Electrochem. Commun.*, 2010, **12**, 1662-1665.
23 L.-Y. Lin, C.-P. Lee, R.Vittal and K.-C. Ho, *J. Power Sources*, 2011, **196**, 1671-1676.
24 M. Matlosz, P. H. Vallotton, A. C. West and D. Landolt, *J. Electrochem. Soc.* , 1992, **139**, 752-761.
25 S. R. Ye, A. R. Rathmell, Z. F. Chen, I. E. Stewart and B. J. Wiley, *Adv. Mater.*, 2014, **26**, 6670-6687.

26 P. Joshi, L. Zhang, Q. Chen, D. Galipeau, H. Fong and Q. Qiao, *ACS Appl. Mater. Interfaces*, 2010, **2**, 3572-3577.

27 H. Wu, L. Hu, M. W. Rowell, D. Kong, J. J. Cha, J. R. McDonough, J. Zhu, Y. Yang, M. D. McGehee and Y. Cui, *Nano Lett.*, 2010, **10**, 4242-4248.

28 H. Wu, D. Kong, Z. Ruan, P.-C. Hsu, S. Wang, Z. Yu, T. J. Carney, L. Hu, S. Fan and Y. Cui, *Nat. Nanotechnol.*, 2013, **8**, 421-425.

29 W. Guo, C. Chen, M. Ye, M. Lv and C. Lin, *Nanoscale*, 2014, **6**, 3656-3663.

30 K. Sun, B. H. Fan and J. Y. Ouyang, *J. Phys. Chem. C*, 2010, **114**, 4237-4244.

31 A. I. Popov and D. H. Geske, *J. Am. Chem. Soc.*, 1958, **80**, 1340-1352.

32 Z. Huang, X. Liu, K. Li, D. Li, Y. Luo, H. Li, W. Song, L. Chen and Q. Meng, *Electrochem. Commun.* , 2007, **9**, 596-598.